Comparing Jupiter interior structure models to *Juno* gravity measurements and the role of a dilute core

S. M. Wahl[1], W. B. Hubbard[2], B. Militzer[1,3], T. Guillot[4], Y. Miguel[4], Y. Kaspi[5], R. Helled[6,7], , D. Reese[8], N. Movshovitz[9,6], E. Galanti[5], S. Levin[10], J.E. Connerney[11], S.J. Bolton[12]

[1]Department of Earth and Planetary Science, University of California, Berkeley, CA, 94720, USA

[2]Lunar and Planetary Laboratory, The University of Arizona, Tucson, AZ 85721, USA

[3]Department of Astronomy, University of California, Berkeley, CA, 94720, USA

[4] Laboratoire Lagrange, UMR 7293, Université de Nice-Sophia Antipolis, CNRS, Observatoire de la Côte dAzur, CS 34229, 06304 Nice Cedex 4, France

[5]Department of Earth and Planetary Sciences, Weizmann Institute of Science, Rehovot, Israel.

[6]Department of Geophysics, Atmospheric, and Planetary Sciences Tel-Aviv University, Israel

[7]Institute for Computational Sciences, University of Zurich, Zurich, Switzerland

[8]LESIA, Observatoire de Paris, France

[9]Department of Astronomy and Astrophysics, University of California, Santa Cruz, CA 95064, USA

[10]JPL, Pasadena, CA, 91109, USA

[11]NASA/GSFC, Greenbelt, MD, 20771, USA

[12]SwRI, San Antonio, TX, 78238, USA

Key Points:

- Precise gravity measurements allow better predictions of interior structure and core mass.
- Juno's gravity measurements imply an increase in the abundance of heavy elements deep in the planet, at or inside of its metallic region.
- The inferred structure includes a dilute core, expanded to a significant fraction of Jupiter's radius.

Corresponding author: Sean M. Wahl, swahl@berkeley.edu

Abstract

The *Juno* spacecraft has measured Jupiter's low-order, even gravitational moments, J_2–J_8, to an unprecedented precision, providing important constraints on the density profile and core mass of the planet. Here we report on a selection of interior models based on *ab initio* computer simulations of hydrogen-helium mixtures. We demonstrate that a dilute core, expanded to a significant fraction of the planet's radius, is helpful in reconciling the calculated J_n with *Juno*'s observations. Although model predictions are strongly effected by the chosen equation of state, the prediction of an enrichment of Z in the deep, metallic envelope over that in the shallow, molecular envelope holds. We estimate Jupiter's core to contain an 7–25 Earth mass of heavy elements. We discuss the current difficulties in reconciling measured J_n with the equations of state, and with theory for formation and evolution of the planet.

1 Introduction

The *Juno* spacecraft entered an orbit around Jupiter in July of 2016, and has begun measuring since then has measured Jupiter's gravitational field to high precision [*Bolton et al.*, 2017]. Here we present a preliminary suite of interior structure models for comparison with the low order gravitational moments (J_2, J_4, J_6 and J_8) measured by *Juno* during its first two perijoves [*Folkner*, 2017].

A well constrained interior structure is a primary means of testing models for the formation of the giant planets. The abundance and distribution of elements heavier than helium (subsequently referred to as "heavy elements") in the planet is key in relating gravity measurements to formation processes. In the canonical model for the formation of Jupiter, a dense core composed $\sim$10 $M_\oplus$ (Earth masses) of rocky and icy material forms first, followed by a period of rapid runaway accretion of nebular gas [*Mizuno et al.*, 1978; *Bodenheimer and Pollack*, 1986; *Pollack et al.*, 1996]. Recent formation models suggest that even in the core accretion scenario, the core can be small ($\sim$ 2 $M_\oplus$) or be diffused with the envelope [*Venturini et al.*, 2016; *Lozovsky et al.*, 2017]. If Jupiter formed by gravitational instability, i.e., the collapse of a region of the disk under self-gravity [*Boss*, 1997], there is no requirement for a core, although a core could still form at a later stage [*Helled et al.*, 2014]. Even if the planet initially formed with a distinct rock-ice core, at high pressures and temperatures these core materials become soluble in liquid metallic hydrogen

[*Stevenson*, 1985; *Wilson and Militzer*, 2012a,b; *Wahl et al.*, 2013; *Gonzalez et al.*, 2013]. As a result, the core will erode and the heavy material will be redistributed outward to some extent. In this study we consider the effect of such a dilute core, in which the heavy elements have expanded to a significant fraction of Jupiter's radius.

Significant progress has been made in understanding hydrogen-helium mixtures at planetary conditions [*Saumon et al.*, 1995; *Saumon and Guillot*, 2004; *Vorberger et al.*, 2007; *Militzer and Hubbard*, 2008; *Fortney and Nettelmann*, 2010; *Nettelmann et al.*, 2012; *Militzer*, 2013; *Becker et al.*, 2013; *Militzer et al.*, 2016], but interior model predictions are still sensitive to the hydrogen-helium equation of state used [*Hubbard and Militzer*, 2016; *Miguel et al.*, 2016]. In Section 2.1 we describe the derivation of barotropes from a hydrogen-helium equation of state based on *ab-initio* materials simulations [*Militzer*, 2013; *Hubbard and Militzer*, 2016], make comparison's to other equations of states, and consider simple perturbations to better understand their affect on the models. In Section 2.2 we describe details of these models including a predicted layer of ongoing helium rain-out [*Stevenson and Salpeter*, 1977a,b; *Morales et al.*, 2009; *Lorenzen et al.*, 2009; *Wilson and Militzer*, 2010; *Morales et al.*, 2013], with consideration of a dilute core in Section 2.3. We then describe the results of these models in therms of their calculated J_n (Section 3.2) and heavy element mass and distribution (Section 3.3). Finally, in Section 4 we discuss these results in relation to the present state of measurements of, as well as theory for the formation and evolution of Jupiter.

2 Materials and Methods

2.1 Barotropes

In this paper we consider interior density profiles in hydrostatic equilibrium,

$$\nabla P = \rho \nabla U, \tag{1}$$

where P is the pressure and ρ is the mass density. In order to find a consistent density profile, we use a barotrope $P(\rho)$ corresponding to isentropic profiles constructed from various equations of state.

Most of the results presented are based on density functional theory molecular dynamics (DFT-MD) simulations of hydrogen-helium mixtures from *Militzer* [2013] and *Militzer and Hubbard* [2013] (MH13). For densities below those determined by the *ab*

initio simulations ($P < 5$ GPa), we use the *Saumon et al.* [1995] equation of state (SCvH), which has been used extensively in giant planet modeling. The benefits of this simulation technique lie in its ability to determine the behavior of mixture through the metallization transition, and to directly calculate entropy for the estimation of adiabtic profiles. The barotropes are parameterized in terms of helium and heavy element mass fraction Y and Z, and specific entropy S as a proxy for the adiabatic temperature profile; for additional details see Supplementary Section S1.

For comparison, we consider models using the *ab initio* equations of state of hydrogen and helium calculated by *Becker et al.* [2013](REOS3) with the procedure for estimating the entropy described by *Miguel et al.* [2016]. Finally, we also consider models using the SCvH EOS through the entire pressure range of the planet. Although the SCvH EOS does not fit the most recent data from high-pressure shockwave experiments [*Hubbard and Militzer*, 2016; *Miguel et al.*, 2016], it is a useful for comparison given since it has been used to constrain Jupiter models in the past [e.g. *Saumon and Guillot*, 2004].

Different equations of state affect model outcomes in part by placing constraints on the allowable abundance and distribution of heavy elements. The DFT-MD isentrope consistent with the *Galileo* probe measurements has higher densities, and a less steep isentropic temperature profile than SCvH in the vicinity of the metallization transition [*Militzer*, 2013; *Militzer et al.*, 2016]. The H-Reos equation of state has a similar shape to the $T(P)$ profile, but has an offset in temperature of several hundred K through much of the molecular envelope [*Nettelmann et al.*, 2012; *Hubbard and Militzer*, 2016; *Miguel et al.*, 2016].

DFT-MD simulation is currently the best technique at present for determining densities of hydrogen-helium mixtures over most of conditions in a giant planet ($P > 5$ GPa). There is, however, a poorly characterized uncertainty in density for DFT-MD calculations. Shock-wave experiments are consistent with DFT, but can only test their accuracy to, at best ~6 % [*Knudson et al.*, 2004; *Brygoo et al.*, 2015]. Moreover, there is a necessary extrapolation between ~5 GPa, where the simulations become too computationally expensive [*Militzer*, 2013; *Militzer and Hubbard*, 2013], and ~10 bar where the deepest temperature measurements from the *Galileo* probe were obtained [*Seiff et al.*, 1997]. We consider perturbations to the MH13 equation of state in the form of an entropy jump, ΔS, at a prescribed pressure in the outer, molecular envelope; Increases of S from 7.07 up to

117 7.30 (with S in units of Boltzmann constant per electron) are considered. These perturba-
118 tions test the effect of a density decrease through the entire envelope (P =0.01 GPa), at
119 the switch from SCvH to DFT (5.0 GPa), and near the onset of the metalization transition
120 (50.0 GPa).

121 Gravitational moments for the models are calculated using the non-perturbative con-
122 centric Maclaurin spheroid (CMS) method [*Hubbard*, 2012, 2013; *Hubbard and Militzer*,
123 2016; *Wahl et al.*, 2016]; see Supplementary Section S2 for additional details.

124 **2.2 Model assumptions**

125 One of the most significant structural features of Jupiter's interior arises from a
126 pressure-induced immiscibility of hydrogen and helium, which allows for rain-out of he-
127 lium from the planet's exterior to interior [*Stevenson and Salpeter*, 1977a,b]. *Ab initio* sim-
128 ulations [*Morales et al.*, 2009; *Lorenzen et al.*, 2009; *Wilson and Militzer*, 2010; *Morales*
129 *et al.*, 2013] predict that the onset of this immiscibility occurs around ∼100 GPa, over a
130 similar pressure range as the molecular to metallic transition in hydrogen. At higher pres-
131 sures, the miscibility gap closure temperature remains nearly constant with pressure, such
132 that in the deep interior temperatures are sufficient for helium to become miscible again.

133 The MH13 adiabats cross the *Morales et al.* [2013] phase diagram such that helium
134 rain-out occurs between ∼100-300 GPa [*Militzer et al.*, 2016]. This is consistent with the
135 sub-solar Y measurement made by the *Galileo* entry probe [*von Zahn et al.*, 1998]. The
136 REOS3 adiabats are significantly warmer and require adjustments to the phase diagram in
137 order to explain the observations [*Nettelmann et al.*, 2015]. Although the detailed physics
138 involved with the formation and growth of a helium rain layer is poorly understood [*Fort-*
139 *ney and Nettelmann*, 2010], the existence of a helium rain layer has a number of important
140 consequences for the thermal and compositional structure of the planet.

141 We calculate the abundance of helium in the both the upper helium-poor (molecular
142 hydrogen) region and lower helium-rich (metallic hydrogen) region by enforcing a helium
143 to hydrogen ratio that is globally protosolar. We also allow for a compositional gradient
144 of heavy elements across the layer with a mass mixing ratio that changes from Z_1 in the
145 lower layer to Z_2 in the upper layer.

2.3 Dilute Core

The thermodynamic stability of various material phases in giant planet interiors has been assessed using DFT-MD calculations [*Wilson and Militzer*, 2012a,b; *Wahl et al.*, 2013; *Gonzalez et al.*, 2013]. These calculations suggest that at the conditions at the center of Jupiter, all likely abundant dense materials will dissolve into the metallic hydrogen-helium envelope. Thus, a dense central core of Jupiter is expected to be presently eroded or eroding. However, the redistribution of heavy elements amounts to a large gravitational energy cost and the efficiency of that erosion is difficult to assess [see *Guillot et al.*, 2004]. It was recently shown by *Vazan et al.* [2016], that redistribution of heavy elements by convection is possible, unless the initial composition gradient is very steep. Some formation models suggest that a gradual distribution of heavy elements is an expected outcome, following the deposition of planetesimals in the gaseous envelope [*Lozovsky et al.*, 2017]. The formation of a compositional gradient could lead to double-diffusive convection [*Chabrier and Baraffe*, 2007; *Leconte and Chabrier*, 2013] in Jupiter's deep interior, which could lead to a slow redistribution of heavy elements, even on planetary evolution timescales.

In a selection of the models presented here, we consider Jupiter's "core" to be a region of the planet in which Z is enriched by a constant factor compared to the envelope region exterior to it. This means that the model core is a diffuse region composed largely of the hydrogen-helium mixture. In fact, this configuration is not very different from the internal structure derived by *Lozovsky et al.* [2017] for proto-Jupiter. Given the current uncertainty in the evolution of a dilute core, we consider models with core in various degrees of expansion, $0.15 < r/r_J < 0.6$. In a few models, we also test the importance of the particular shape of the dilute core profile by considering a core with a Gaussian Z profile instead. Fig. 1 demonstrates the density profiles resulting from these different assumptions about the distribution of core heavy elements.

3 Results

3.1 Comparison to *Juno*

The even zonal moments observed by *Juno* after the first two perijoves [*Folkner*, 2017] are broadly consistent with the less precise predictions of *Campbell and Synnott* [1985] and *Jacobson* [2003], but inconsistent with the more recent JUP310 solution [*Ja-*

cobson, 2013]. Table 1 compares these observations with a few representative models. Although the solid-body (static) contribution dominates this low-order, even part of the gravity spectrum [*Hubbard*, 1999], a small dynamical contribution above *Juno*'s expected sensitivity must be considered [*Kaspi et al.*, 2010]. For sufficiently deep flows, these contributions could be many times larger than *Juno*'s formal uncertainties for J_n [*Kaspi et al.*, 2017], and thus represent the conservative estimate of uncertainty for the purpose of constraining the interior structure. Thus, ongoing gravity measurements by *Juno*, particularly of odd and high order, even J_n, will continue to improve our understanding of Jupiter's deep interior [*Kaspi*, 2013]. Marked in yellow in Fig 2, is the possible uncertainty considering a wide range of possible flows, and finding a corresponding density distribution assuming the large scale flows are to leading order geostrophic [*Kaspi et al.*, 2009]. The relatively small range in our model J_6 and J_8 compared to these uncertainties suggests flow in Jupiter are shallower than the most extreme cases considered by *Kaspi et al.* [2017].

3.2 Model Trends

It is evident that the J_n observed by *Juno* are not consistent with the "preferred" model put forward by *Hubbard and Militzer* [2016], even considering differential rotation. Nonetheless, we begin with a similar model (Model A in Tab. 1) since it is illustrative of the features of the model using the MH13 equation of state with reasonable pre-*Juno* estimates for model parameters. A detailed description of the reference model is included Supplementary Section S3.

In order to increase J_4 for a given planetary radius and J_2, show that one needs to either increase the density below the 100 GPa pressure level or conversely decrease the density above that level [*Guillot*, 1999, their Fig. 5]. We explore two possibilities: either we raise the density in the metallic region by expanding the central core, or we consider the possibility of an increased entropy in the molecular region.

Fig. 2 shows the effect of increasing the radius of the dilute core on J_4 and J_6. Starting with the MH13 reference model with $r/r_J = 0.15$ (Model A), the core radius is increased incrementally to $r/r_J \sim 0.4$, above which the model becomes unable to fit J_2. Therefore, considering an extended core shifts the higher order moments in the towards the *Juno* values, but is unable to reproduce J_4, even considering a large dynamical contribution to J_n. Supplementary Fig. S1 shows a similar trend for J_8, although the relative

change in J_8 with model parameters compared to the observed value is less significant than for J_4 and J_6.

Precisely matching *Juno*'s value for J_4 with the MH13 based models presented here, requires lower densities than the reference model through at least a portion of the outer, molecular envelope. In the absence of additional constraints, this can be accomplished by lowering Y or Z, or by increasing S (and consequently the temperature). In Fig. 2 this manifests itself as a nearly linear trend in J_4 and J_6 (black '+' symbols), below which there are no calculated points. This trend also improves the agreement of J_4 and J_6 with *Juno* measurements, but with a steeper slope in J_6/J_4 than that from the dilute core. For $\Delta S \sim 0.14$ applied at P =0.01 GPa, a model with this perturbed equation of state can match the observed J_4, with a mismatch in J_6 of $\sim 0.1 \times 10^{-6}$ below the observed value (Model F). When the ΔS perturbation is applied at higher pressures ($P = 5.0$ and 50.0 GPa), the larger a ΔS is needed to produce the same change in J_4.

We also consider a number of models with both a decrease in the density of the outer, molecular layer and a dilute core. Here we present MH13 models where the core radius is increased for models with outer envelope $Z = 0.010$, 0.007 or 0.0. Above $Z \sim 0.010$ the models are unable to simultaneously match J_2 and J_4. The models with $Z = 0.010$ and $Z = 0.007$ can both fit J_4, but with a $J_6 \sim 0.1 \times 10^{-6}$ above the observed value (Models C & D). These models also require extremely dilute cores with $r/r_J \sim 0.5$ in order to match J_4. A more extreme model with no heavy elements ($Z = 0$) included in the outer, molecular envelope (Model B) can simultaneously match J_4 and J_6 within the current uncertainty, with a less expansive core with $r/r_J \sim 0.27$. The dilute core using the Gaussian profile and an outer envelope $Z = 0.007$ (Model E), has a very similar trend in J_4–J_6, although it is shifted to slightly lower values of J_6.

There are a number of other model parameters which lead to similar, but less pronounced, trends than the dilute core. Starting with Model C, we test shifting the onset pressure for helium rain, between 50 to 200 GPa, and the entropy in the deep interior, $S = 7.07$ to 7.30 (lower frame in Fig. 2). Both modifications exhibit a similar slope in J_4–J_6 to the models with different core radii, but spanning a smaller range in J_4 than for the dilute core trend.

The models using REOS3 have a significantly hotter adiabatic T profile than MH13. Models R and S (1) are two example solutions obtained with the REOS3 adiabat, for a

3-layer model with a compact core, and when adding a dilute core, respectively. Because of the flexibility due to the larger Z values that are required to fit Jupiter's mean density, there are a wide range of solutions [*Nettelmann et al.*, 2012; *Miguel et al.*, 2016] with J_4 values that can extend all the way from -599 to -586×10^{-6}, spanning the range of values of the MH13 solutions. Model T corresponds to a model calculated with the same ΔZ discontinuity at the molecular-metallic transition as Model S but with a compact instead of dilute core. This shows that, as in the case of the MH13 EOS, with all other parameters fixed, a dilute core yields larger J_4 values.

For both DFT-based equations of state, we find that heavy element abundances must increase in the planet's deep interior. The required ΔZ across the helium rain layer is increased when hotter REOS3 equation of state, and decreased by considering a dilute core. Regardless of the EOS used, including a diffuse core has a similar effect on J_6, increasing the value by a similar amount for similar degree of expansion, when compared to an analogous model with a compact core. Thus J_6 may prove to be a useful constraint in assessing the degree of expansion of Jupiter's core.

3.3 Predicted Core Mass

Fig. 3 displays the total mass of heavy elements, along with the proportion of that mass in the dilute core. Models using MH13 with dilute cores, have core masses between 10 and 24 $M_\oplus$ (Earth masses), with gradual increase from 24 to 27 $M_\oplus$ for the total heavy elements in the planet. Of the models able to fit the observed J_4, those with heavy element contents closer to the *Galileo* value have more extended cores containing a greater mass of heavy elements.

The perturbation of the equation of state with an entropy jump, has an opposite effect on the predicted core mass with respect to the dilute core, despite the similar effect on the calculated J_n. For increasingly large ΔS perturbations, core mass decreases, to $\sim$8 $M_\oplus$, while total heavy element mass increases. As this perturbation is shifted to higher pressures the change in core mass becomes less pronounced, for a given value of ΔZ. In all the cases considered here, the MH13 equation of state predicts significantly larger core masses and lower total heavy element mass than the SCvH equation of state.

All of the models depicted in Fig. 3 represent fairly conservative estimates of the heavy element mass. For any such model, there is a trade-off in densities that can be in-

troduced where the deep interior is considered to be hotter (higher S), and that density deficit is balanced by a higher value of Z. It is also possible, that a dilute core would introduce a superadiabatic temperature profile, which would allow for a similar trade-off in densities and additional mass in the dilute core. Constraining this requires an evolutionary model to constrain the density and temperature gradients through the dilute core [*Leconte and Chabrier*, 2012, 2013], and has not been considered here. Shifting the onset pressure of helium rain can shift the core mass by $\sim$2 $M_\oplus$ in either direction If the majority of the heavy core material is denser rocky phase [*Soubiran and Militzer*, 2016], the corresponding smaller value of ρ_0/ρ_Z results in a simultaneous decrease in core mass and total Z of $\sim$2–4 $M_\oplus$.

Using the REOS3, both models with a small, compact core of $\sim$6 $M_\oplus$ or a diluted core of $\sim$19 $M_\oplus$ are possible, along with a continuum of intermediate solutions. These models have a much larger total mass of heavy elements, 46 and 34 $M_\oplus$, a direct consequence of the higher temperatures of that EOS [see *Miguel et al.*, 2016]. The enrichment in heavy elements over the solar value in the molecular envelope correspond to about 1 for model R and 1.4 for model S, pointing to a water abundance close to the solar value in the atmosphere of the planet. In spite of the difference in total mass of heavy element, the relationship between core mass and radius is similar for MH13 and REOS3.

In lieu of additional constraints we can likely bracket the core mass between 6–25 $M_\oplus$, with larger masses corresponding to more dilute profile of the core. These masses for the dilute core are broadly consistent those required by the core-collapse formation model *Pollack et al.* [1996], as well as models that account for the dissolution of planetesimals [*Lozovsky et al.*, 2017]. The mass of heavy element in the envelope, and thus the total heavy element mass is strongly affected by the equation of state, with MH13 predicting 5–6$\times$ solar fraction of total heavy elements in Jupiter and REOS3 around $7-10\times$ solar fraction.

4 Conclusion

After only two perijoves the *Juno* gravity science experiment has significantly improved the measurements of the low order, even gravitational moments J_2–J_8 [*Folkner*, 2017]. The formal uncertainty on these measured J_n is already sufficiently small that they would be able to distinguish small differences between interior structure models, assuming

that the contribution to these low order moments arises primarily from the static interior density profile. Considering a wide range of possible dynamical contributions increases the effective uncertainty of the static J_2–J_8 by orders of magnitude [*Kaspi et al.*, 2017]. It is expected that the dynamical contribution to J_n will be better constrained following future perijove encounters by the *Juno* spacecraft with measurements of odd and higher order even J_n [*Kaspi*, 2013].

Even with this greater effective uncertainty, it is possible to rule out a portion of the models presented in this study, primarily on the basis on the observed J_4. The reference model, using a DFT-MD equation of state with direct calculation of entropy in tandem with a consistent hydrogen-helium phase-diagram is incompatible with a simple interior structure model constrained by composition and temperature from the *Galileo* entry probe.

Our models suggest that a dilute core, expanded through a region 0.3–0.5 times the planet's radius is helpful for fitting the observed J_n. Moreover, for a given J_4 the degree to which the core is expanded affects J_6 and J_8 in a predictable, model independent manner, such that further constraining J_6 and J_8 may allow one to determine whether Jupiter's gravity requires such an dilute core. Such a core might arise through erosion of an initially compact rock-ice core, or through a differential rate of planetesimal accretion during growth, although both present theoretical challenges.

Using the REOS3 approach leads to a wider range of possibilities which include solutions with the standard 3-layer model approach or assuming the presence of a dilute core. In any case, as for the MH13 solutions, the REOS3 solutions require the abundance of heavy elements to increase in the deep envelope. This indicates that Jupiter's envelope has not been completely mixed.

These results present a challenge for evolutionary modelling of Jupiter's deep interior [e.g. *Vazan et al.*, 2016; *Mankovich et al.*, 2016]. The physical processes involved with the formation and stability of a dilute core are not understood. It strongly depends on the formation process of the planet and the mixing at the early stages after formation, and also enters a hydrodynamical regime of double diffusive convection where competing thermal and compositional gradients can result in inefficient mixing of material [*Leconte and Chabrier*, 2012; *Mirouh et al.*, 2012]. The timescale for the formation and evolution of such features, especially on planetary length scales is still poorly understood. In particular, it is not known whether there would be enough convective energy to expand 10 $M_\oplus$

or more of material to 0.3 to 0.5× Jupiter's radii. It is also presently unknown whether it is plausible to expand the core to this degree without fully mixing the entire planet, and without resorting to extremely fortuitous choices in parameters. Since Jovian planets are expected to go through periods of rapid cooling shortly after accretion [*Fortney and Nettelmann*, 2010], if they are mostly convective, it is likely that much of the evolution of an dilute core would have to occur early on in the planet's history when the convective energy is greatest. This presents a challenge for explaining interior models requiring a large ΔZ across the helium rain layer, as such a would form after the period of most intense mixing.

In our preliminary models, those able to fit J_4 have lower densities in portions of the outer molecular envelope than MH13. These be achieved though modifying abundances of helium and heavy elements to be than those measured by the *Galileo* entry probe, or invoking a hotter non-adiabatic temperature profile. Some formation scenarios [e.g. *Mousis et al.*, 2012] can account for relatively low envelope H_2O content ($\sim$ 2× solar), but our models would require even more extreme depletions if for this to be explained by composition alone. Alternatively there might be an overestimation of the density inherent to the DFT simulations of MH13 by on the order of ∼3% for $P < 100$

Interior models could, therefore, be improved through further theoretical and experimental studies of hydrogen-helium mixtures, particularly in constraining density in the pressure range below ∼100 GPa, where the models are most sensitive to changes in equation of state. More complicated equation of state perturbations, including the onset and width of the metallization transition [*Knudson and Desjarlais*, 2017] may be worth considering in future modelling efforts. Similarly, the interior modeling effort will be aided by an independent measurement of atmospheric H_2O from *Juno*'s microwave radiometer (MWR) instrument [*Helled and Lunine*, 2014].

Acknowledgments

This work was supported by NASA's Juno project. SW and BM acknowledge the support the National Science Foundation (Astronomy and Astrophysics Research Grant 1412646). TG and YM acknowledge support from CNES. We acknowledge the helpful input and discussion from Johnathan Lunin, David Stevenson, William Folkner and the *Juno* Interiors Working Group.

Table 1. Comparison of selected models to observed gravitational moments

	Model Description[a]	Z_1[c]	Z_2	J_2	J_4	J_6	J_8	J_{10}	C/Ma^2	$r_{\rm core}/r_J$	$M_{\rm core}$	$M_{Z,\rm env}$	$M_{Z,\rm total}$	$Z_{\rm global}$
	Juno observed[b]			−14696.514	−586.623	34.244	−2.502							
				±0.272	±0.363	±0.236	±0.311							
A	MH13, $Z_{\rm Gal}$, compact core	0.0169	0.0298	14696.641	-594.511	34.998	-2.533	0.209	0.26391	0.150	13.2	10.5	23.6	0.0744
B	MH13, dilute core	0.0000	0.0451	14696.641	-586.577	34.196	-2.457	0.202	0.26400	0.270	10.4	13.9	24.2	0.0762
C	MH13, dilute core	0.0100	0.0114	14696.467	-586.613	34.360	-2.481	0.205	0.26396	0.498	18.5	7.3	25.8	0.0812
D	MH13, dilute core	0.0071	0.0199	14696.641	-586.585	34.392	-2.486	0.205	0.26396	0.530	21.3	5.1	26.4	0.0831
E	MH13, Gaussian core	0.0071	0.0087	14696.467	-586.588	34.336	-2.479	0.204	0.26397	–	23.5	3.3	26.8	0.0843
F	Perturbed MH13, compact core	0.0169	0.0526	14696.466	-586.588	34.117	-2.444	0.200	0.26400	0.150	9.3	15.9	25.1	0.0791
G	SCvH, compact core	0.0820	0.0916	14696.641	-587.437	34.699	-2.541	0.212	0.26393	0.150	1.5	32.7	34.2	0.1076
R	REOS3, compact core	0.0131	0.1516	14696.594	-586.631	34.186	-2.457	0.202	0.26443	0.110	6.21	40.0	46.2	0.1454
S	REOS3, dilute core	0.0209	0.0909	14696.755	-586.658	34.346	-2.480	0.204	0.26442	0.533	19.2	14.5	33.7	0.1061
T	REOS3, compact core, low J_4	0.0293	0.0993	14696.381	-593.646	34.933	-2.529	0.209	0.26432	0.122	8.9	27.0	35.9	0.1129

[a] Equation of state used, dilute or compact core, $Z_{\rm Gal}$ denotes model with Z_1 matching *Galileo* probe measurement. [b] *Folkner* [2017].

[c] Z_1 denotes the heavy element fraction in molecular envelope, Z_2 denotes heavy element fraction in the metallic envelope, but exterior to the core.

Confidential manuscript submitted to *Geophysical Research Letters*

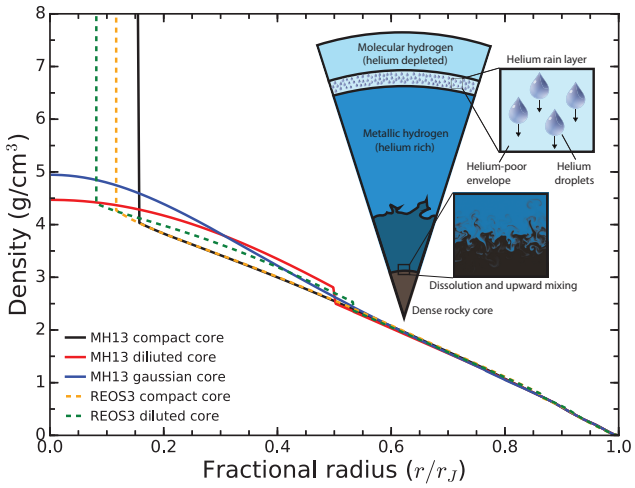

Figure 1. Density profiles of representative models. Solid lines denote models using MH13, while dashed use REOS3. In black is a model with S, Y and Z matching that measured by the *Galileo* entry probe, and a core with constant enrichment of heavy elements inside r/r_J=0.15. In red (Model D) Z=0.007 in the molecular envelope and constant Z-enriched, dilute core expanded to $r/r_J \sim 0.50$ to fit the J_4 observed by *Juno*. In blue (Model E) with Z=0.007 also fitting J_4 with Gaussian Z profile. In orange (Model X) and green (Model Y) are profiles for the REOS3 models fitting J_4 with a compact and dilute core, respectively. (Inset) Schematic diagram showing the approximate location of the helium rain layer, and dilute core.

References

Becker, A., N. Nettelmann, B. Holst, and R. Redmer (2013), Isentropic compression of hydrogen: Probing conditions deep in planetary interiors, *Phys. Rev. B - Condens. Matter Mater. Phys.*, *88*(4), 1–7, doi:10.1103/PhysRevB.88.045122.

Bodenheimer, P., and J. B. Pollack (1986), Calculations of the accretion and evolution of giant planets: The effects of solid cores, *Icarus*, *67*(3), 391–408, doi:10.1016/0019-1035(86)90122-3.

Bolton, S. J., A. Adriani, V. Adumitroaie, J. Anderson, and S. Atreya (2017), Jupiter's Interior and Deep Atmosphere, *Science*.

Boss, A. P. (1997), Giant Planet Formation by Gravitational Instability, *Science (80-.).*, *276*(5320), 1836–1839, doi:10.1126/science.276.5320.1836.

Brygoo, S., M. Millot, P. Loubeyre, A. E. Lazicki, S. Hamel, T. Qi, P. M. Celliers, F. Coppari, J. H. Eggert, D. E. Fratanduono, D. G. Hicks, J. R. Rygg, R. F. Smith, D. C. Swift, G. W. Collins, R. Jeanloz, S. Brygoo, M. Millot, P. Loubeyre, A. E. Laz-

icki, S. Hamel, T. Qi, P. M. Celliers, F. Coppari, J. H. Eggert, D. E. Fratanduono, D. G. Hicks, J. R. Rygg, R. F. Smith, D. C. Swift, G. W. Collins, and R. Jeanloz (2015), Analysis of laser shock experiments on precompressed samples using a quartz reference and application to warm dense hydrogen and helium, *J. Appl. Phys.*, *118*, 195,901, doi:10.1063/1.4935295.

Campbell, J., and S. Synnott (1985), Gravity field of the Jovian system from Pioneer and Voyager tracking data, *Astron. J.*, *90*, 364–372, doi:10.1086/113741.

Chabrier, G., and I. Baraffe (2007), Heat Transport in Giant (Exo)planets: A New Perspective, *Astrophys. J.*, *661*(1), L81—-L84, doi:10.1086/518473.

Folkner, W. M. (2017), PreliminaryJuno Gravity Results, *Geophys. Res. Lett.*, *(This issu*.

Fortney, J., and N. Nettelmann (2010), The Interior Structure, Composition, and Evolution of Giant Planets, *SSR*, *152*, 423.

Gonzalez, F., H. F. Wilson, and B. Militzer (2013), Solubility of silica in metallic hydrogen: implications to rocky core solubility of giant planets, *Phys. Rev. B*.

Guillot, T. (1999), Interiors of giant planets inside and outside the solar system., *Science (80-.).*, *286*(5437), 72–7.

Guillot, T., D. J. Stevenson, W. B. Hubbard, and D. Saumon (2004), The interior of Jupiter, *In: Jupiter. The planet*, p. 35.

Helled, R., and J. Lunine (2014), Measuring Jupiter's water abundance by Juno: The link between interior and formation models, *Mon. Not. R. Astron. Soc.*, *441*(3), 2273–2279, doi:10.1093/mnras/stu516.

Helled, R., P. Bodenheimer, M. Podolak, A. Boley, F. Meru, S. Nayakshin, J. J. Fortney, L. Mayer, Y. Alibert, and A. P. Boss (2014), Giant Planet Formation, Evolution, and Internal Structure., in *Protostars Planets VI, Henrik Beuther, Ralf S. Klessen, Cornelis P. Dullemond, Thomas Henning*, pp. 914 pp., p.643–665, University of Arizona Press, Tuscon.

Hubbard, W. B. (1999), Gravitational Signature of Jupiter's Deep Zonal Flows, *Icarus*, *137*(2), 357–359, doi:http://dx.doi.org/10.1006/icar.1998.6064.

Hubbard, W. B. (2012), High-Precision Maclaurin-Based Models of Rotating Liquid Planets, *Astrophys. J.*, *756*(1), L15, doi:10.1088/2041-8205/756/1/L15.

Hubbard, W. B. (2013), Concentric Maclaurin Spheroid Models of Rotating Liquid Planets, *Astrophys. J.*, *768*(1), 43, doi:10.1088/0004-637X/768/1/43.

Hubbard, W. B., and B. Militzer (2016), A Preliminary Jupiter Model, *Astrophys. J.*, *820*(80).

Jacobson, R. A. (2003), JUP230 orbit solution.

Jacobson, R. A. (2013), JUP310 Orbit Solution.

Kaspi, Y. (2013), Inferring the depth of the zonal jets on Jupiter and Saturn from odd gravity harmonics, *Geophys. Res. Lett.*, *40*(4), 676–680, doi:10.1029/2012GL053873.

Kaspi, Y., G. R. Flierl, and A. P. Showman (2009), The deep wind structure of the giant planets: Results from an anelastic general circulation model, *Icarus*, *202*(2), 525–542, doi:10.1016/j.icarus.2009.03.026.

Kaspi, Y., W. B. Hubbard, A. P. Showman, and G. R. Flierl (2010), Gravitational signature of Jupiter's internal dynamics, *Geophys. Res. Lett.*, *37*, L01,204, doi:10.1029/2009GL041385.

Kaspi, Y., T. Guillot, E. Galanti, Y. Miguel, and R. Helled (2017), The effect of differential rotation on Jupiter's low-order even gravity moments, *Geophys. Res. Lett.*, *(This issu*.

Knudson, M. D., and M. P. Desjarlais (2017), High-Precision Shock Wave Measurements of Deuterium : Evaluation of Exchange-Correlation Functionals at the Molecular-to-Atomic Transition, *Phys Rev Lett*, *118*(035501), doi:10.1103/PhysRevLett.118.035501.

Knudson, M. D., D. L. Hanson, J. E. Bailey, C. A. Hall, J. R. Asay, and C. Deeney (2004), Principal Hugoniot, reverberating wave, and mechanical reshock measurements of liquid deuterium to 400 GPa using plate impact techniques, *Phys. Rev. B - Condens. Matter Mater. Phys.*, *69*(14), 1–20, doi:10.1103/PhysRevB.69.144209.

Leconte, J., and G. Chabrier (2012), A new vision of giant planet interiors: Impact of double diffusive convection, *Astron. Astrophys.*, *540*(ii), A20, doi:10.1051/0004-6361/201117595.

Leconte, J., and G. Chabrier (2013), Layered convection as the origin of Saturn's luminosity anomaly, *Nat. Geosci.*, *6*(April), 347–350, doi:10.1038/ngeo1791.

Lorenzen, W., B. Holst, and R. Redmer (2009), Demixing of hydrogen and helium at megabar pressures, *Phys. Rev. Lett.*, *102*, 115,701, doi:10.1103/PhysRevLett.102.115701.

Lozovsky, M., R. Helled, E. D. Rosenberg, P. Bodenheimer, and E. P. Jan (2017), Jupiter's formation and its primordial internal structure, *ApJ (in Press.*, pp. 1–31.

Mankovich, C., J. J. Fortney, and K. L. Moore (2016), Bayesian Evolution Models for Jupiter With Helium Rain and Double-Diffusive Convection, *Astrophys. J.*, *832*(2), 113,

469 doi:10.3847/0004-637X/832/2/113.

470 Miguel, Y., T. Guillot, and L. Fayon (2016), Jupiter internal structure: the effect of differ-
471 ent equations of state.

472 Militzer, B. (2013), Equation of state calculations of hydrogen-helium mix-
473 tures in solar and extrasolar giant planets, *Phys. Rev. B*, *87*(1), 014,202, doi:
474 10.1103/PhysRevB.87.014202.

475 Militzer, B., and W. Hubbard (2008), A massive core in Jupiter predicted from first-
476 principles simulations, *Astrophys. . . .*, (Militzer), 2006–2009.

477 Militzer, B., and W. B. Hubbard (2013), Ab Initio Equation of State for Hydrogen-Helium
478 Mixtures With Recalibration of the Giant-Planet Mass-Radius Relation, *Astrophys. J.*,
479 *774*(2), 148, doi:10.1088/0004-637X/774/2/148.

480 Militzer, B., F. Soubiran, S. M. Wahl, and W. Hubbard (2016), Understanding Jupiter 's
481 interior, *J. Geophys. Res. Planets*, *121*, 1552–1572, doi::10.1002/2016JE005080.

482 Mirouh, G. M., P. Garaud, S. Stellmach, A. L. Traxler, and T. S. Wood (2012), a New
483 Model for Mixing By Double-Diffusive Convection (Semi-Convection). I. the Condi-
484 tions for Layer Formation, *Astrophys. J.*, *750*(1), 61, doi:10.1088/0004-637X/750/1/61.

485 Mizuno, H., K. Nakazawa, and C. Hayashi (1978), Instability of a Gaseous Envelope Sur-
486 rounding a Planetary Core and Formation of Giant Planets, *Prog. Theor. Phys.*, *60*(3),
487 699–710.

488 Morales, M. A., E. Schwegler, D. Ceperley, C. Pierleoni, S. Hamel, and K. Caspersen
489 (2009), Phase separation in hydrogen-helium mixtures at Mbar pressures., *Proc. Natl.*
490 *Acad. Sci. U. S. A.*, *106*(5), 1324–9, doi:10.1073/pnas.0812581106.

491 Morales, M. a., S. Hamel, K. Caspersen, and E. Schwegler (2013), Hydrogen-helium
492 demixing from first principles: From diamond anvil cells to planetary interiors, *Phys.*
493 *Rev. B*, *87*(17), 174,105, doi:10.1103/PhysRevB.87.174105.

494 Mousis, O., J. I. Lunine, N. Madhusudhan, and T. V. Johnson (2012), Nebular Water De-
495 pletion As the Cause of Jupiter'S Low Oxygen Abundance, *Astrophys. J. Lett.*, *751*, L7,
496 doi:10.1088/2041-8205/751/1/L7.

497 Nettelmann, N., A. Becker, B. Holst, and R. Redmer (2012), Jupiter Models With Im-
498 proved Ab Initio Hydrogen Equation of State (H-Reos.2), *Astrophys. J.*, *750*(1), 52, doi:
499 10.1088/0004-637X/750/1/52.

500 Nettelmann, N., J. J. Fortney, K. Moore, and C. Mankovich (2015), An exploration of
501 double diffusive convection in Jupiter as a result of hydrogen-helium phase separation,

Mon. Not. R. Astron. Soc., *447*, 3422–3441, doi:10.1093/mnras/stu2634.

Pollack, J. B., O. Hubicky, P. Bodenheimer, and J. J. Lissauer (1996), Formation of the Giant Planets by Concurrent Accretion of Solids Gas, *Icarus*, *124*, 62–85, doi:10.1006/icar.1996.0190.

Saumon, D., and T. Guillot (2004), Shock Compression of Deuterium and the Interiors of Jupiter and Saturn, *Astrophys. J.*, *609*(2), 1170–1180, doi:10.1086/421257.

Saumon, D., G. Chabrier, and H. M. van Horn (1995), An equation of state for low-mass stars and giant planets, *ApJSS*, *99*, 713.

Seiff, A., D. B. Kirk, T. Knight, L. A. Young, and F. Sohl (1997), Thermal Structure of Jupiter's Upper Atmosphere Derived from the Galileo Probe, *Science (80-.).*, *276*(5309), 102–104, doi:10.1126/science.276.5309.102.

Soubiran, F., and B. Militzer (2016), The properties of heavy elements in giant planet envelopes, *Astrophys. J.*, *829*, 14, doi:10.3847/0004-637X/829/1/14.

Stevenson, D. (1985), Cosmochemistry and structure of the giant planets and their satellites, *Icarus*, *62*, 4–15, doi:10.1016/0019-1035(85)90168-X.

Stevenson, D. J., and E. E. Salpeter (1977a), The phase diagram and transport properties for hydrogen-helium fluid planets, *Astrophys. J. Suppl. Ser.*, *35*, 221, doi:10.1086/190478.

Stevenson, D. J., and E. E. Salpeter (1977b), Dynamics and helium distribution in hydrogen-helium fluid planets, *Astrophys. J. Suppl. Ser.*, *35*, 239.

Vazan, A., R. Helled, M. Podolak, and A. Kovetz (2016), the Evolution and Internal Structure of Jupiter and Saturn With Compositional Gradients, *Astrophys. J.*, *829*(2), 118, doi:10.3847/0004-637X/829/2/118.

Venturini, J., Y. Alibert, and W. Benz (2016), Planet formation with envelope enrichment: new insights on planetary diversity, *Astron. Astrophys.*, *496*(id.A90), 14, doi:10.1051/0004-6361/201628828.

von Zahn, U., D. M. Hunten, and G. Lehmacher (1998), Helium in Jupiter's atmosphere: Results from the Galileo probe helium interferometer experiment, *J. Geophys. Res.*, *103*, 22,815–22,829.

Vorberger, J., I. Tamblyn, B. Militzer, and S. Bonev (2007), Hydrogen-helium mixtures in the interiors of giant planets, *Phys. Rev. B*, *75*(2), 024,206, doi:10.1103/PhysRevB.75.024206.

Wahl, S. M., H. F. Wilson, and B. Militzer (2013), Solubility of Iron in Metallic Hydrogen and Stability of Dense Cores in Giant Planets, *Astrophys. J.*, *773*(2), 95, doi: 10.1088/0004-637X/773/2/95.

Wahl, S. M., W. B. Hubbard, and B. Militzer (2016), The Concentric Maclaurin Spheroid method with tides and a rotational enhancement of Saturn's tidal response, *Icarus (in Rev.*

Wilson, H. F., and B. Militzer (2010), Sequestration of noble gases in giant planet interiors., *Phys. Rev. Lett.*, *104*(12), 121,101.

Wilson, H. F., and B. Militzer (2012a), Solubility of Water Ice in Metallic Hydrogen: Consequences for Core Erosion in Gas Giant Planets, *Astrophys. J.*, *745*(1), 54, doi: 10.1088/0004-637X/745/1/54.

Wilson, H. F., and B. Militzer (2012b), Rocky Core Solubility in Jupiter and Giant Exoplanets, *Phys. Rev. Lett.*, *108*(11), 111,101, doi:10.1103/PhysRevLett.108.111101.

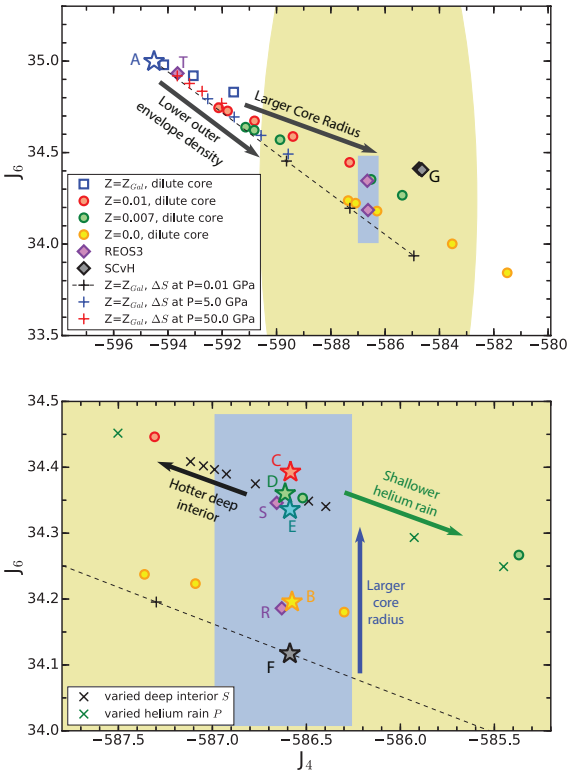

Figure 2. Zonal gravitational moments J_4 and J_6 for interior models matching the measured J_2. (Upper) The blue rectangle shows the uncertainty of the *Juno* measurements as of perijove 2 [*Folkner*, 2017]. The yellow region shows the effective uncertainty in the static contribution due possible deep differential rotation [*Kaspi et al.*, 2017]. The blue star is the reference (Model A) with S, Y and Z matching that measured by the *Galileo* entry probe, and an core of r/r_J=0.15. The blue squares show how these results change as a dilute core with a constant Z enrichment with increasing r is considered. The green and red circles denote similar expanding core trends with lowered outer envelope heavy element fraction to Z=0.007 and Z=0.01, respectively. The '+'s denote models which take perturb the MH13 EOS by introducing a jump in S at P=0.01 (black), P=5.0 (blue) and P=50.0 GPa (red). Black diamonds show models using the SCvH EOS at all conditions. (Lower) The stars denote models B,C,D,E, & F in Table 1. Violet diamonds show models using the REOS3 EOS (Models X and Y). Black and green 'x's show models starting with the green star (dilute core, Z=0.007) and changing the S of the deep interior or the onset pressure of helium rain. Red, green and cyan stars show models fitting the measured J_4 with the radius of the dilute core. Black Star shows model fitting J_4 with with the entropy jump magnitude ΔS.

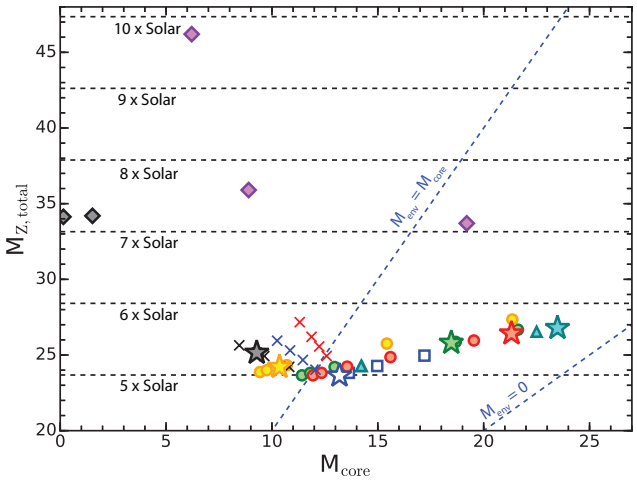

Figure 3. Mass of heavy elements in the core of the model versus the total heavy element mass in Jupiter predicted by the model. Symbols refer to identical models as in Fig 2. The stars denote models included in Table 1. Horizontal lines display the values of $M_{\mathrm{Z,total}}$, corresponding to 5, 6, 7 and 8× solar abundance of heavy elements.

Supporting Information for

"Comparing Jupiter interior structure models to *Juno* gravity measurements and the role of an expanded core"

S. M. Wahl[1], W. B. Hubbard[2], B. Militzer[1,3], T. Guillot[4], Y. Miguel[4], Y. Kaspi[5], R. Helled[6,7], , D. Reese[8], N. Movshovitz[9,6], E. Galanti[5], S. Levin[10], J.E. Connerney[11], S.J. Bolton[12]

[1]Department of Earth and Planetary Science, University of California, Berkeley, CA, 94720, USA

[2]Lunar and Planetary Laboratory, The University of Arizona, Tucson, AZ 85721, USA

[3]Department of Astronomy, University of California, Berkeley, CA, 94720, USA

[4] Laboratoire Lagrange, UMR 7293, Université de Nice-Sophia Antipolis, CNRS, Observatoire de la Côte dAzur, CS 34229, 06304 Nice Cedex 4, France

[5]Department of Earth and Planetary Sciences, Weizmann Institute of Science, Rehovot, Israel.

[6]Department of Geophysics, Atmospheric, and Planetary Sciences Tel-Aviv University, Israel

[7]Institute for Computational Sciences, University of Zurich, Zurich, Switzerland

[8]LESIA, Observatoire de Paris, France

[9]Department of Earth and Planetary Sciences, University of California, Santa Cruz, CA 95064, USA

[10]JPL, Pasadena, CA, 91109, USA

[11]NASA/GSFC, Greenbelt, MD, 20771, USA

[12]SwRI, San Antonio, TX, 78238, USA

Contents

S1. Equations of State

The *ab initio* simulations for MH13 were performed at a single, solar-like helium mass fraction, $Y_0 = 0.245$. The precise abundance and distribution for both helium and heavy element fractions are, *a priori* unknown. These are quantified in terms of their local mass fractions, Y and Z. Our models consider different proportions of both components by perturbing the densities using a relation derived from the additive value law [*Hubbard and Militzer*, 2016]. For the helium density we use the pure helium end-member of SCvH. We assume a density ratio of heavy element to hydrogen helium mixture, ρ_0/ρ_Z, of 0.38

Corresponding author: Sean M. Wahl, swahl@berkeley.edu

for pressures below 100 GPa, corresponding to heavy element composition measured by the *Galileo* entry probe [*Wong et al.*, 2004], and 0.42 for a solar fraction at higher pressures; see discussion in *Hubbard and Militzer* [2016]. The MH13 equation of state uses density functional theory molecular dynamics (DFT-MD) simulations in combination with a thermodynamic integration to find the entropy of the simulated material. This allows one to directly characterize an adiabat for the *ab initio* equation of state as the $T(P)$ path in which the simulated entropy per electron $S/k_B/N_e$ remains constant. Here k_B is Boltzmann's constant and N_e is the number of electrons. In the following discussion, the term "entropy" and the symbol S are used interchangeably to refer to the particular adiabatic temperature profile through regions of the planet presumed to be undergoing efficient convection. In this work, we assume that the compositional perturbations have a negligible effect on the isentropic temperature profile [*Soubiran and Militzer*, 2016].

Models calculated with REOS3 followed the approach described by *Miguel et al.* [2016]: We fitted separately the core mass and composition in heavy elements. The helium content of the molecular region was fixed to the Galileo value while the increase in helium abundance in the metallic region was calculated to reproduce the protosolar value. The abundance of heavy elements was allowed to be different in the molecular and metallic regions.

1 S2. Calculation of Gravitational Moments

The unprecedented precision of *Juno*'s gravity measurements presents a challenge, as they are more precise than the perturbative methods historically used to calculate J_n from an interior structure model, [e.g. *Zharkov and Trubitsyn*, 1978]. For the results presented here, we instead use the non-perturbative, *concentric Maclaurin spheroid* (CMS) method [*Hubbard*, 2012, 2013; *Hubbard and Militzer*, 2016; *Wahl et al.*, 2016]. In this method, the density structure is parameterized by N nested, constant-density spheroids and the gravitational field is calculated as a volume-integrated function of all of the spheroids. The method uses an iterative approach to find the shape of each spheroid, such that the surface of each follows an equipotential surface of the total effective potential, U, from the planet's self-gravity and the rotation. The result is a model with a self-consistent shape, internal density distribution and gravitational field. The method has been shown to be precise and efficient, and has been benchmarked against an independent, non-perturbative method [*Wisdom and Hubbard*, 2016].

The CMS models presented here parameterize the spheroid radii using progressively smaller Δr from deep to shallow. The outermost layer has a Δr of 1 km in thickness, which allows the model to resolve the density structure consistent with $P = 1$ bar at the outer surface. We use an axisymmetric version of the CMS method with 510 spheroids, and a spherical harmonic expansion up to order $n = 16$.

S3. Reference Interior Model

The reference model (model A) fixes parameters in the outer (molecular) envelope to those measured by the *Galileo* entry probe: $S = 7.074$, $Y = 0.2333$ and $Z = 0.0169$. It should be noted that the Z from *Galileo* is based on a measurement showing sub-solar ratio of H_2O to other ices (i.e. CH_4 and NH_3) [*Wong et al.*, 2004]. It has been hypothesized that the entry probe may have descended through an anomalously dry region of Jupiter's atmosphere, in which case this value of Z may be an underestimate. The helium ratio of the deep (metallic) envelope is chosen assuming that the *Galileo* Y was depleted from a solar composition by helium rain , and the deep entropy is chosen as a moderate enhancement across the helium rain layer, $S = 7.13$. An upper and lower pressure of the helium rain layer are determined by finding where the two adiabatic profiles for the inner and outer envelope intersect the [*Morales et al.*, 2013] phase diagram. This step is done self-consistently for all values of S, except in a few extreme cases where the corresponding adiabat does not intersect the phase diagram.

The interior structures of the REOS3 models presented here differ in the treatment of the helium rain, assuming a 3-layer boundary with a sharp transition between the molecular and metallic envelopes. The difference J_6 between the REOS3 model with the compact core (model X) and the perturbed EOS (model F) can be attributed to this structural difference.

The MH13 models assume that the helium-rain layer is superadiabatic, a natural consequence of inefficient convection [*Militzer et al.*, 2016]. In the case of the REOS3 models, because the adiabat is significantly warmer, the presence of such a superadiabatic region has minor quantitative consequences on the solutions and was not considered. In that case, we used the approach described in *Miguel et al.* [2016].

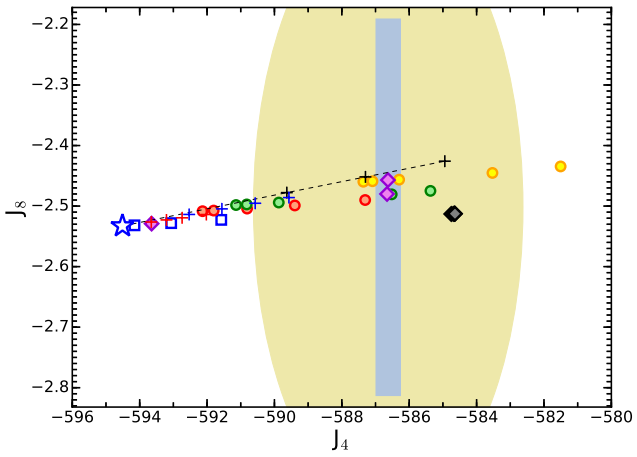

Figure S1. Zonal gravitational moments J_4 and J_8 for interior models matching the measured J_2. The rectangles show the uncertainty of the *Juno* measurements as of perijove 2 [*Folkner*, 2017].The yellow region shows the effective uncertainty in the static contribution due possible deep differential rotation [*Kaspi et al.*, 2017]. Symbols refer to identical models as in Fig. 2 in the main text.

References

Folkner, W. M. (2017), PreliminaryJuno Gravity Results, *Geophys. Res. Lett.*, *(This issu*.

Hubbard, W. B. (2012), High-Precision Maclaurin-Based Models of Rotating Liquid Planets, *Astrophys. J.*, *756*(1), L15, doi:10.1088/2041-8205/756/1/L15.

Hubbard, W. B. (2013), Concentric Maclaurin Spheroid Models of Rotating Liquid Planets, *Astrophys. J.*, *768*(1), 43, doi:10.1088/0004-637X/768/1/43.

Hubbard, W. B., and B. Militzer (2016), A Preliminary Jupiter Model, *Astrophys. J.*, *820*(80).

Kaspi, Y., T. Guillot, E. Galanti, Y. Miguel, and R. Helled (2017), The effect of differential rotation on Jupiter's low-order even gravity moments, *Geophys. Res. Lett.*, *(This issu*.

Miguel, Y., T. Guillot, and L. Fayon (2016), Jupiter internal structure: the effect of different equations of state.

Militzer, B., F. Soubiran, S. M. Wahl, and W. Hubbard (2016), Understanding Jupiter 's interior, *J. Geophys. Res. Planets*, *121*, 1552–1572, doi::10.1002/2016JE005080.

Morales, M. a., S. Hamel, K. Caspersen, and E. Schwegler (2013), Hydrogen-helium demixing from first principles: From diamond anvil cells to planetary interiors, *Phys. Rev. B*, *87*(17), 174,105, doi:10.1103/PhysRevB.87.174105.

Soubiran, F., and B. Militzer (2016), The properties of heavy elements in giant planet envelopes, *Astrophys. J.*, *829*, 14, doi:10.3847/0004-637X/829/1/14.

Wahl, S. M., W. B. Hubbard, and B. Militzer (2016), The Concentric Maclaurin Spheroid method with tides and a rotational enhancement of Saturn's tidal response, *Icarus (in Rev.*

Wisdom, J., and W. B. Hubbard (2016), Differential rotation in Jupiter: A comparison of methods, *Icarus*, *267*, 315–322, doi:10.1016/j.icarus.2015.12.030.

Wong, M. H., P. R. Mahaffy, S. K. Atreya, H. B. Niemann, and T. C. Owen (2004), Updated Galileo probe mass spectrometer measurements of carbon, oxygen, nitrogen, and sulfur on Jupiter, *Icarus*, *171*, 153–170, doi:10.1016/j.icarus.2004.04.010.

Zharkov, V. N., and V. P. Trubitsyn (1978), *The physics of planetary interiors*, 380 pp., Parchart, Tucson, AZ.